Supplementary material

Detailed information about the morphological and flow characteristics of each healthy subject and the averaged models are provided in this Supplementary document for the manuscript entitled "Computational analysis of blood flow in healthy pulmonary arteries in comparison to repaired Tetralogy of Fallot results: a small cohort study" by Boumpouli et al.

Flow information

Table S1 presents the diameters, mean flow rate and mean and maximum velocities for the 5 healthy subjects and the anatomical averaged model.

Table S1. Analysis of the MPA, RPA and LPA branches of each model. The diameters, mean flow rate, and mean and maximum velocities are provided for the 5 healthy subjects and the anatomical averaged geometry.

Healthy Subject	1	2	3	4	5	Anatomical Average
D_{MPA} (m)	0.028	0.027	0.030	0.029	0.032	0.028
D_{RPA} (m)	0.018	0.020	0.022	0.024	0.020	0.017
D_{LPA} (m)	0.019	0.019	0.021	0.021	0.021	0.017
Q_{mean} (ml/s)	98.7	75.7	100.2	78.3	78.6	86.3
$U_{meanMPA}$ (m/s)	0.161	0.133	0.145	0.117	0.098	0.161
$U_{meanRPA}$ (m/s)	0.213	0.129	0.138	0.094	0.106	0.196
$U_{meanLPA}$ (m/s)	0.160	0.130	0.146	0.109	0.127	0.179
U_{maxMPA} (m/s)	0.495	0.417	0.553	0.466	0.382	0.493
U_{maxRPA} (m/s)	0.652	0.404	0.526	0.371	0.411	0.689
U_{maxLPA} (m/s)	0.490	0.407	0.557	0.432	0.493	0.632

Morphological analysis

The individual values of curvature, tortuosity, min sphere radius, in-plane and out-of-plane anles are presented in Tables S2 and S3 for the 5 healthy subjects and the anatomical averaged model. In addition, to further extend the morphological analysis, Table S2 presents the values of torsion, $\tau(s)$, which quantifies the divergence of a curve from lying on the oscillation plane [1], $\tau(s)=([c'(s) \times c''(s)] \cdot c'''(s))/\| c'(s) \times c(s) \|$.

Table S2. Morphological analysis of the curvature and torsion for the 5 healthy subjects and the anatomical averaged geometry. The mean value and standard deviation (SD) are based on the analysis of all six geometries (5 patients and anatomical averaged).

Healthy Subject	Curvature RPA (mm^{-1}) (mean / max)	Curvature LPA (mm^{-1}) (mean / max)	Torsion RPA (mm^{-1}) (min / mean / max)	Torsion LPA (mm^{-1}) (min / mean / max)
1	0.018 / 0.063	0.014 / 0.046	-1.59 / 0.00 / 0.57	-1.63 / 0.00 / 0.45
2	0.017 / 0.063	0.015 / 0.062	-1.08 / 0.00 / 1.63	-2.02 / 0.04 / 0.59

3	0.018 / 0.057	0.015 / 0.053	-0.98 / 0.00 / 0.54	-0.49 / -0.03 / 0.51
4	0.019 / 0.093	0.020 / 0.093	-1.08 / -0.03 / 0.37	-1.13 / 0.22 / 0.65
5	0.016 / 0.062	0.017 / 0.068	-0.29 / 0.00 / 0.15	-4.33 / -0.7 / 0.10
Anatomical Averaged	0.024 / 0.077	0.020 / 0.048	-1.40 / 0.01 / 0.88	-0.20 / 0.04 / 0.67

Table S3. Morphological analysis of the tortuosity, minimum inscribed sphere radius along the daughter branches, and in-plane and out-of-plane angles for the 5 healthy subjects and the anatomical averaged geometry. The mean value and standard deviation (SD) are based on the analysis of all six geometries.

Healthy Subject	Tortuosity (RPA/LPA)	Min Sphere Radius (mm) (RPA/LPA)	In-Plane angles (RPA/LPA)	Out-of-Plane Angles (RPA/LPA)
1	0.073 / 0.080	8.36 / 7.90	142.9° / 152.2°	-0.6° / 17°
2	0.114 / 0.100	8.39 / 5.79	136.6° / 131.8°	3.0° / -1.9°
3	0.092 / 0.154	9.20 / 8.62	137.2° / 149.1°	-7.1° / -10.5°
4	0.066 / 0.126	10.27 / 8.82	134.3° / 115.6°	8.8° / -24.9°
5	0.069 /0.113	9.09 / 8.79	141.0° / 144.6°	6.0° / -17.7°
Anatomical Averaged	0.095 / 0.089	7.3 / 7.5	139.8° / 132.5°	-6.3° / 18.4°

Figure S1 shows the decrease of the maximum inscribed sphere radius along the centerlines of the LPA (Figure S1A) and RPA branches (Figure S1B) of the healthy geometries. The curvilinear abscissa was again normalized, as in the curvature plots (Figure 4 of the main paper). A steep decrease in the sphere radius was observed in both cases at the entrance of the pulmonary bifurcation, which was more pronounced in the LPA branch. A larger variability in the sphere radius of the geometries was observed for the RPA branch distal to the bifurcation.
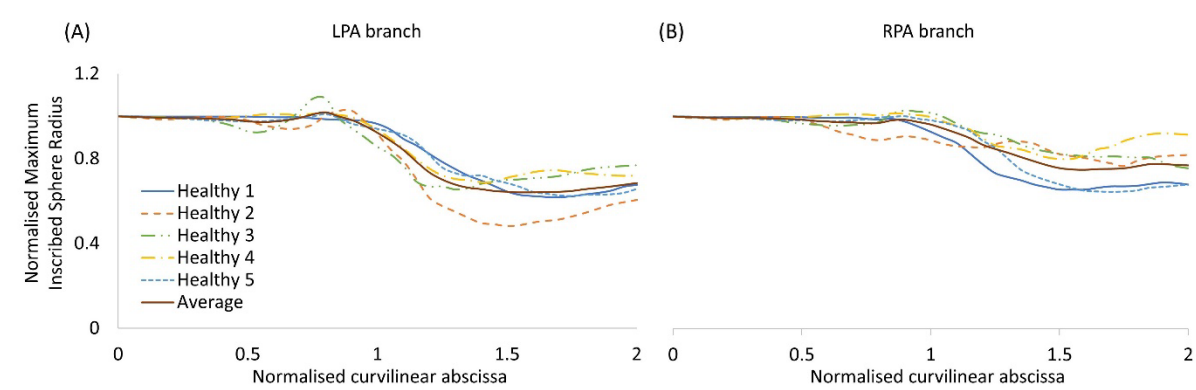

Figure S1. Change of the maximum inscribed sphere radius along the (A) LPA and (B) RPA branch. X-axis is normalized based on the maximum inscribed sphere radius at the level of the MPA inlet. Y- axis is normalized

with the value corresponding to the peak curvature (closer to the bifurcation) of each geometry, similar to Figure 4 of the paper.

Dimensionless numbers

The individual values of the mean and max Reynolds, De_{max} and Womersley numbers for the 5 healthy subjects and the anatomical averaged model are presented in Table S4. In general, Re_{mean}, Re_{max}, De_{max} and Wo numbers did not vary greatly within the healthy geometries and similar values were observed between the right and left pulmonary arteries.

Table S4. Flow analysis of the subject-specific models. The Reynolds (Re), Dean (De) and Womersley (Wo) numbers are provided for the 5 healthy subjects and the anatomical averaged geometry. The mean value and standard deviation (SD) are based on the analysis of all six geometries.

Healthy Subject	Re_{mean_MPA} (Re_{max_MPA})	Re_{mean_RPA} (Re_{max_RPA})	Re_{mean_LPA} (Re_{max_LPA})	De_{max_RPA}	De_{max_LPA}	Wo
1	1199 (3678)	1032 (3165)	790 (2423)	1179	885	21.6
2	952 (2977)	684 (2138)	644 (2012)	1027	882	21.0
3	1141 (4365)	804 (3076)	792 (3029)	1673	1468	21.0
4	907 (3598)	595 (2362)	591 (2347)	1241	1391	19.8
5	831 (3237)	572 (2228)	707 (2752)	1033	1573	20.6
Anatomical Averaged	1199 (3666)	888 (3121)	815 (2871)	1547	1129	21.6

Non-dimensionalized streamlines of velocity

Velocity streamlines at three time points, peak flow (Figure S2.I), mid-deceleration during systole (Figure S2.II), and mid-diastole (Figure S2.III), are presented in Figure S2 non-dimensionalized. The three time-points are also indicated on the subject-specific and the average waveforms which are provided on the left side of the figure. At peak systole, slightly higher velocities were developed at the entrance of the RPA branch and in the opening of the LPA in all geometries (Figures S2A.I-F.I). Increased velocity was noticed at the RPA for geometries 1, 4 and the averaged geometry (Figures S2A.I, S2D.I, S2F.I), and at the LPA of geometries 2 and 5 (Figures S2B.I, S2E.I). During deceleration (Figure S2.II), the largest recirculation zones appeared in the RPA of geometries 2 and 4 (Figures S2B.II, S2D.II), while smaller areas of recirculation of flow were visible at the entrance of the LPA, in all geometries (Figures S2A.II-F.II). Finally, more complex patterns appeared during mid diastole (Figure S2.III), and especially in the pulmonary junction of geometries 1, 2, 4 and the averaged geometry (Figures S2A.III, S2B.III, S2D.III, S2F.III). The averaged geometry in general captured well the main characteristics of the flow development in the healthy pulmonary arteries.
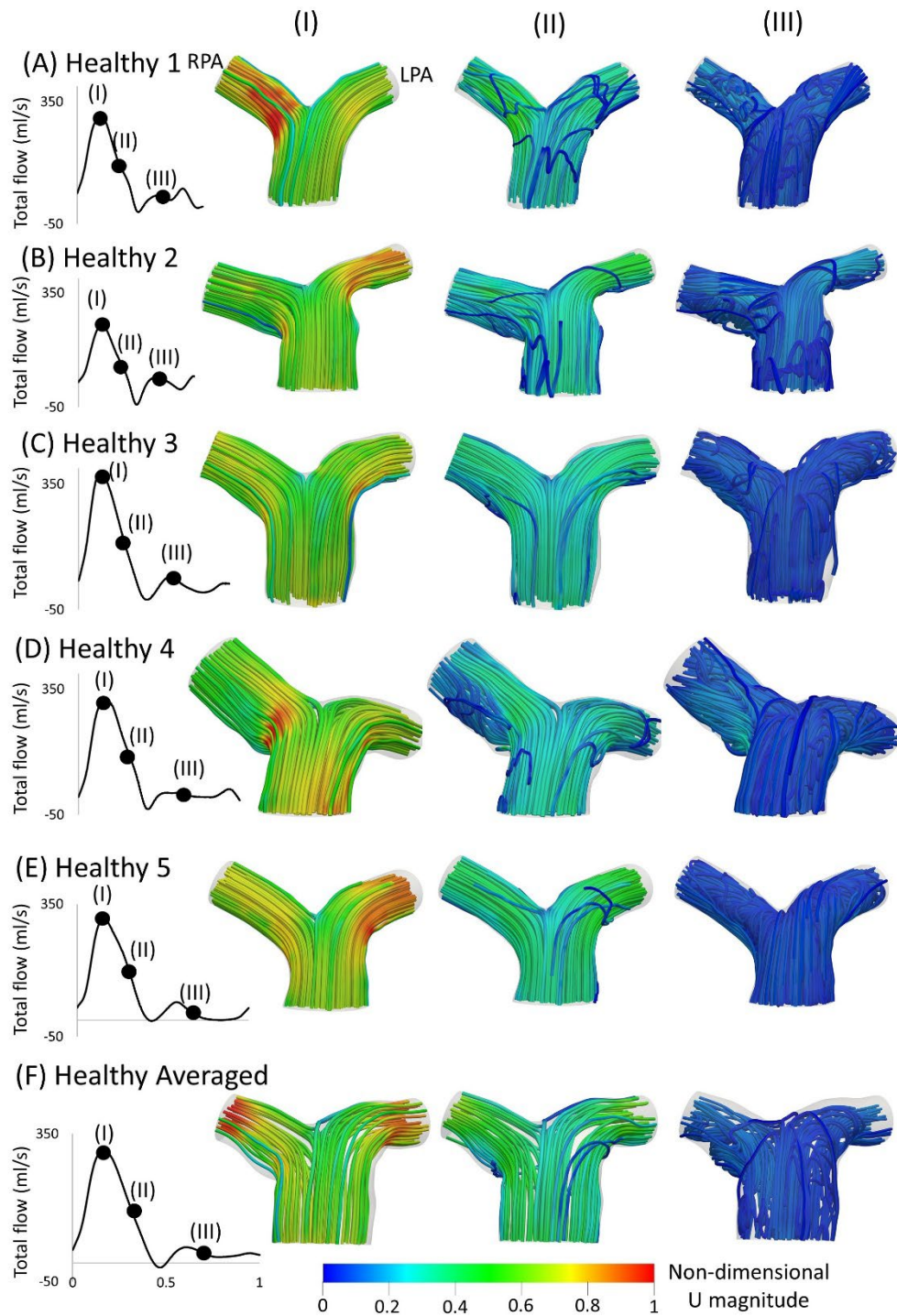
Figure S2. Subject-specific flow waveforms for the healthy (A) 1; (B) 2; (C) 3; (D) 4; (E) 5 geometries, and (F) the healthy anatomical averaged geometry, at (I) peak flow, (II) mid-deceleration at systole, and (III) mid-diastole, respectively. Streamlines of velocity are also presented, colored by non-dimensionalized velocity. Non-dimensionalization is based on division with the maximum velocity corresponding to each healthy subject. The RPA and the LPA branches are indicated in (A.I).

Secondary flows

The secondary flows displayed in the cross sections (α) and (γ) in the healthy pulmonary arterial models 1, 2 and 4 indicate that there is not much disturbance of flow during peak flow (Figure S3). A small vortex was visible in the RPA branch of the healthy 1 model, while a stable focus was visible in the healthy 4 model.
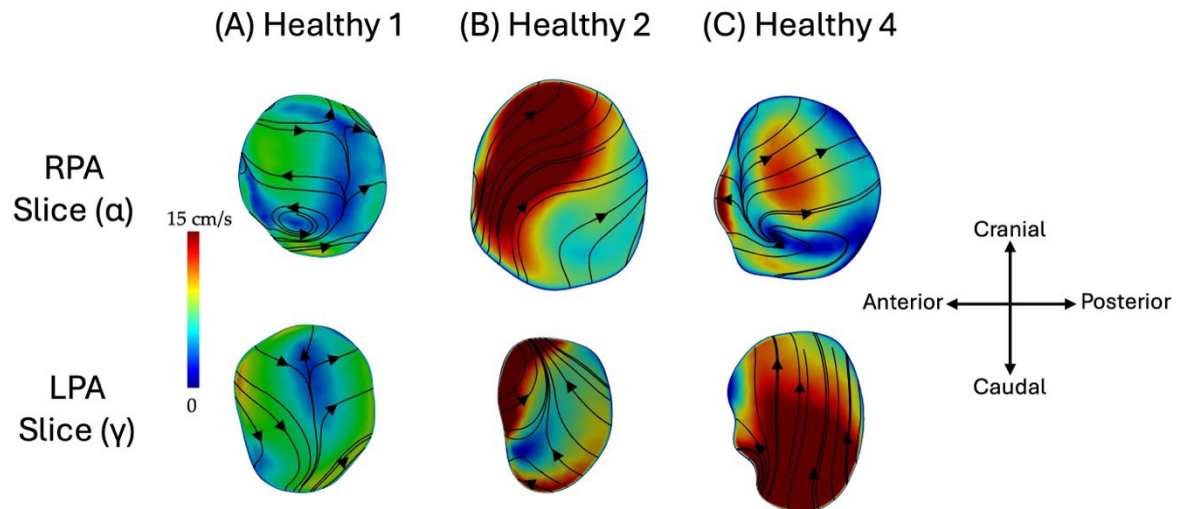

Figure S3: Secondary flows visualised by in-plane velocity vectors, at slices (α) and (γ), during peak flow, for the (A) healthy 1; (B) healthy 2; and (C) healthy 4 models.

References

1. Piccinelli, M.; Veneziani, A.; Steinman, D.A.; Remuzzi, A.; Antiga, L. A framework for geometric analysis of vascular structures: Application to cerebral aneurysms. IEEE Transactions on medical imaging 1987, 28, 1141-1155. DOI: 10.1109/TMI.2009.2021652.